

NASA Technical Paper 3445

Effects of Isotope Selection on Solution Convergence in HZE Transport

Myung-Hee Y. Kim

The College of William and Mary • Williamsburg, Virginia

John W. Wilson

Langley Research Center • Hampton, Virginia

Richard L. Kiefer

The College of William and Mary • Williamsburg, Virginia

Sheila A. Thibeault

Langley Research Center • Hampton, Virginia

National Aeronautics and Space Administration
Langley Research Center • Hampton, Virginia 23681-0001

May 1994

Introduction

As an analytic solution to the heavy-ion transport equation in terms of Green's function representing nuclear and atomic/molecular processes, a heavy-ion transport code including a database has been provided for laboratory ion beam applications. Results based on the new code were compared with perturbation theory results (ref. 1), which previously had been compared with those of ^{20}Ne transport experiments at the Lawrence Berkeley Laboratory (LBL) BEVALAC accelerator. (See refs. 2 and 3.) In the LBL comparison, the primary errors in the computation were attributed to the nuclear cross sections and the approximations used in applying the acceptance functions. (See ref. 1.) The perturbation code was converted to access the NUCFRAG database (refs. 4 and 5), then a direct comparison between the perturbation code and the nonperturbative Green's function code was made. (See ref. 1.) In this comparison, the sequence of perturbation terms appears to be converging toward the nonperturbative result even though the nonconvergence of the lighter fragments in the first three perturbation terms is clearly apparent. (See ref. 1.) Although the nonperturbative Green's function code eliminates the need to control truncation and discretization errors, it requires further development for comparison with space radiation codes. (See ref. 6.)

Aside from the questions of numerical convergence and convergence of the series solution, the solutions themselves must represent the fields associated with all the isotopes produced in the fragmentation process. In principle, several hundred such isotopes would be required for the transport of iron beams. In practice, only a hundred or so such isotopes contribute to the solution in a significant way. The cosmic ray code that models high-charge and high-energy ions (HZE) and transport (HZETRN) developed at Langley Research Center uses 59 isotopes, whereas many other simulations use only 29. (See refs. 6–8.) Determination of the number of isotopes required for an adequate laboratory beam simulation is the purpose of the present study. In this report, we recall the solution procedures and examine the effects on solution accuracy of representing a reduced set of isotopes. Although we consider only iron beams on epoxy targets, the conclusions are presumed applicable to other target materials and ion beams lighter than iron. This interpretation can be made because the isotopes produced are characterized by the nuclear properties of the fragmented beam particles.

Green's Function for a Single Medium

We restrict our attention to the multiple charged ions for which the Boltzmann equation may be reduced (ref. 6) to

$$\left[\frac{\partial}{\partial x} - \frac{\partial}{\partial E} \tilde{S}_j(E) + \sigma_j \right] \phi_j(x, E) = \sum_k \sigma_{jk} \phi_k(x, E) \quad (1)$$

where $\phi_j(x, E)$ is the ion flux at x with energy E (MeV/amu), $\tilde{S}_j(E)$ is the change in E per unit distance, σ_j is the total macroscopic reaction cross section, and σ_{jk} is the macroscopic cross section for the collision of ion type k to produce an ion of type j . The solution to equation (1) is found subject to the boundary condition

$$\phi_j(0, E) = f_j(E) \quad (2)$$

For this boundary condition, laboratory beams have only one value of j for which $f_j(E)$ is not zero, $f_j(E)$ is described by a mean energy E_o , and the energy spread σ is such that

$$f_j(E) = \frac{1}{\sqrt{2\pi}\sigma} \exp \left[- (E - E_o)^2 / 2\sigma^2 \right] \quad (3)$$

The usual method of solution is to solve equation (1) as a perturbation series. (See refs. 1 and 6.) In practice, the computational requirements limit the usefulness of the technique for deep penetration. (See ref. 3.)

Green's function is introduced as a solution of

$$\left[\frac{\partial}{\partial x} - \frac{\partial}{\partial E} \tilde{S}_j(E) + \sigma_j \right] G_{jm}(x, E, E_o) = \sum_k \sigma_{jk} G_{km}(x, E, E_o) \quad (4)$$

subject to the boundary condition

$$G_{jm}(0, E, E_o) = \delta_{jm} \delta(E - E_o) \quad (5)$$

The solution to equation (1) is given by superposition as

$$\phi_j(x, E) = \sum_k \int G_{jk}(x, E, E') f_k(E') dE' \quad (6)$$

If $G_{jk}(x, E, E')$ is known as an algebraic quantity, the evaluation of equation (6) may be accomplished by simple integration techniques and the associated errors in solving equation (1) numerically are avoided. (See ref. 9.)

The above equations can be simplified by transforming the energy into the residual range as

$$r_j = \int_0^E \frac{dE'}{\tilde{S}_j(E')} \quad (7)$$

and defining new field functions as

$$\psi_j(x, r_j) = \tilde{S}_j(E) \phi_j(x, E) \quad (8)$$

$$\mathcal{G}_{jm}(x, r_j, r'_m) = \tilde{S}_j(E) G_{jm}(x, E, E') \quad (9)$$

$$\hat{f}_j(r_j) = \tilde{S}_j(E) f_j(E) \quad (10)$$

Equation (4) becomes

$$\left[\frac{\partial}{\partial x} - \frac{\partial}{\partial r_j} + \sigma_j \right] \mathcal{G}_{jm}(x, r_j, r'_m) = \sum_k \frac{\nu_j}{\nu_k} \sigma_{jk} \mathcal{G}_{km}(x, r_k, r'_m) \quad (11)$$

with the boundary condition

$$\mathcal{G}_{jm}(0, r_j, r'_m) = \delta_{jm} \delta(r_j - r'_m) \quad (12)$$

and with the solution to the ion fields given by

$$\psi_j(x, r_j) = \sum_m \int_0^\infty \mathcal{G}_{jm}(x, r_j, r'_m) \hat{f}_m(r'_m) dr'_m \quad (13)$$

Note that ν_j is the range scale factor as $\nu_j r_j = \nu_m r_m$ and is taken as $\nu_j = Z_j^2/A_j$. The solution to equation (11) is written as a perturbation series

$$\mathcal{G}_{jm}(x, r_j, r'_m) = \sum_i \mathcal{G}_{jm}^{(i)}(x, r_j, r'_m) \quad (14)$$

where

$$\mathcal{G}_{jm}^{(0)}(x, r_j, r'_m) = g(j) \delta_{jm} \delta(x + r_j - r'_m) \quad (15)$$

and

$$\mathcal{G}_{jm}^{(1)}(x, r_j, r'_m) \approx \frac{\nu_j \sigma_{jm} g(j, m)}{x(\nu_m - \nu_j)} \quad (16)$$

where $\mathcal{G}_{jm}^{(1)}(x, r_j, r'_m)$ is zero unless

$$\frac{\nu_j}{\nu_m}(r_j + x) \leq r'_m \leq \frac{\nu_j}{\nu_m} r_j + x \quad (17)$$

for $\nu_m > \nu_j$. If $\nu_j > \nu_m$, as can happen in neutron removal, the negative of equation (16) is used and the

upper and lower limits of equation (17) are switched. The higher terms are approximated as

$$\begin{aligned} \mathcal{G}_{jm}^{(i)}(x, r_j, r'_m) \approx & \sum_{k_1, k_2, \dots, k_{i-1}} [\nu_j \sigma_{jk_1} \sigma_{k_1 k_2}, \dots, \sigma_{k_{i-1} m} \\ & \times g(j, k_1, k_2, \dots, k_{i-1}, m)] / x(\nu_m - \nu_j) \end{aligned} \quad (18)$$

In the above expression

$$g(j) = e^{-\sigma_j x} \quad (19)$$

and

$$\begin{aligned} g(j_1, j_2, \dots, j_n, j_{n+1}) = & [g(j_1, j_2, \dots, j_{n-1}, j_n) \\ & - g(j_1, j_2, \dots, j_{n-1}, j_{n+1})] / (\sigma_{j_{n+1}} - \sigma_{j_n}) \end{aligned} \quad (20)$$

Note that the terms $\mathcal{G}_{jm}^{(i)}(x, r_j, r'_m)$ are purely dependent on x for $i > 0$, which we represent as $\mathcal{G}_{jm}^{(i)}(x)$. (See ref. 3.) In terms of the above arguments, the solution to equation (1) becomes (ref. 3)

$$\begin{aligned} \psi_j(x, r_j) = & e^{-\sigma_j x} \hat{f}_j(r_j + x) \\ & + \sum_{m,i} \mathcal{G}_{jm}^{(i)}(x) [\hat{F}_m(r'_{ml}) - \hat{F}_m(r'_{mu})] \end{aligned} \quad (21)$$

In equation (21), r'_{ml} and r'_{mu} are given by the lower and upper limits of the inequality in equation (17). The symbol $\hat{F}_m(r'_m)$ refers to the integral spectrum

$$\hat{F}_m(r'_m) = \int_{r'_m}^\infty \hat{f}_m(r) dr \quad (22)$$

We note that

$$\hat{F}_m(r'_m) \equiv F_m(E') \quad (23)$$

with

$$F_m(E') = \int_{E'}^\infty f_m(E) dE \quad (24)$$

and

$$r'_m = \int_0^{E'} \frac{dE}{\tilde{S}_m(E)} \quad (25)$$

We now introduce nonperturbative terms for the summation in equation (21).

First, we recall that the g function of n arguments was generated by the perturbation solution of the

transport equation after neglecting ionization energy loss (ref. 1), which is given by

$$\left(\frac{\partial}{\partial x} + \sigma_j\right)g_{jm}(x) = \sum_k \sigma_{jk}g_{km}(x) \quad (26)$$

subject to the boundary condition

$$g_{jm}(0) = \delta_{jm} \quad (27)$$

for which the solution is

$$g_{jm}(x) = \delta_{jm}g(m) + \sigma_{jm}g(j, m) + \dots \quad (28)$$

The equation

$$g_{jm}(x) = \sum_k g_{jk}(x-y)g_{km}(y) \quad (29)$$

is also true for any positive values of x and y . Equation (29) may be used to propagate the function $g_{jm}(x)$ over the solution space, after which

$$\begin{aligned} \mathcal{G}_{jm}(x, r_j, r'_m) &\approx e^{-\sigma_j x} \delta_{jm} \delta(x + r_j - r'_m) \\ &+ \frac{\nu_j [g_{jm}(x) - e^{-\sigma_j x} \delta_{jm}]}{x(\nu_m - \nu_j)} \end{aligned} \quad (30)$$

The approximate solution of equation (1) is then given by

$$\begin{aligned} \psi_j(x, r_j) &= e^{-\sigma_j x} \hat{f}(r_j + x) \\ &+ \sum_m \frac{\nu_j [g_{jm}(x) - e^{-\sigma_j x} \delta_{jm}]}{x(\nu_m - \nu_j)} \\ &\times [\hat{F}_m(r'_{mu}) - \hat{F}_m(r'_{ml})] \end{aligned} \quad (31)$$

Note that the computational procedures are affected by the size of the number of the elements in equations (28) and (29). The number of terms in the application of equation (29) increases as N^2 , where N is the number of isotope fields represented in the solution given by equation (31). For computational efficiency, the goal is to minimize the number of isotopes without greatly compromising solution accuracy.

Comparison of Isotope Tables

The nonperturbative method generates Green's function for any ion of charge $Z \leq 28$ that results from the impact of that ion on a material medium, including the secondary fragment fields. The atomic weight (taken as the nearest integral value) and

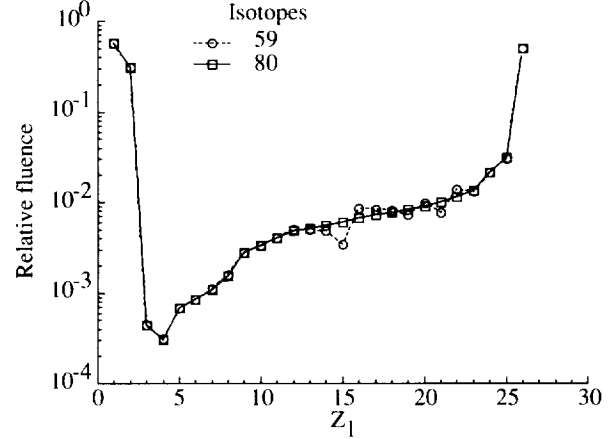


Figure 1. Convergence of charge distribution of 505 MeV/amu iron beams in 5 g/cm² of epoxy for 59 and 80 isotopes.

charge associated with each field function are truncated to the nearest isotope A_l , Z_l in the isotope table. The truncation minimizes the distance to the nearest isotope using the square-distance function

$$D_{il} = (A_i - A_l)^2 + 4(Z_i - Z_l)^2 \quad (32)$$

where A_i , Z_i is the isotope produced in the fragmentation event. Clearly, the accuracy in the transport result requires the isotope list to contain the main isotopes produced in the fragmentation event; the isotopes of lesser importance may be approximated. Initially, 59 isotopes were selected to represent each nuclear mass value between 1 and 58. Such a list was found adequate for the transport of galactic cosmic rays using the HZETRN code. (See refs. 5 and 10.) However, such a representation was inadequate for the transport of an iron beam using the non-perturbative code GRNTRN (ref. 1); thus, more isotopes were added to the table. The total flux of identified projectile fragment nuclei between H and Fe was found for 505 MeV/amu monoenergetic ⁵⁶Fe beams incident on epoxy of 5 g/cm². The resin selected is tetraglycidyl 4,4'-diaminodiphenylmethane (TG 4,4' DDM) epoxy cured with diaminodiphenylsulfone (DDS). A repeat cured unit of epoxy molecular structures is C₃₇H₄₂N₄O₆S and has the density 1.32 g/cm³. Epoxy was applied because it is a more common material and may be fabricated and supplied as a shield medium. The results based on tables of 59 and 80 isotopes are shown in figures 1 and 2. The integral output spectra for the projectiles and fragments in figure 1 show a somewhat similar charge distribution for both 59 and 80 isotopes, but the mass

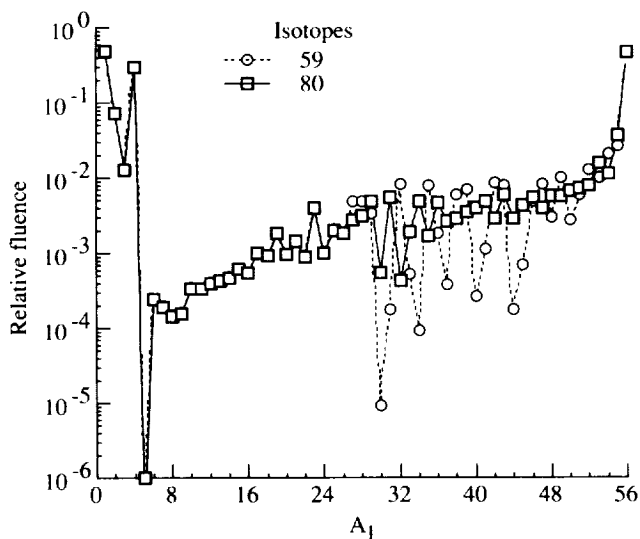


Figure 2. Convergence of mass distribution of 505 MeV/amu iron beams in 5 g/cm² of epoxy for 59 and 80 isotopes.

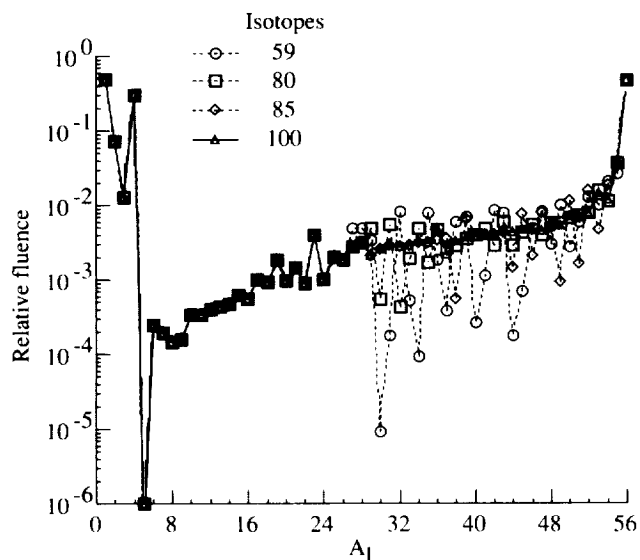


Figure 3. Convergence of mass distribution of 505 MeV/amu iron beams in 5 g/cm² of epoxy for 59, 80, 85, and 100 isotopes.

distributions in figure 2 show large differences. The 80-isotope table is probably adequate for applications in which charge is the dominating factor (e.g., linear energy transfer), but the mass distribution could be substantially improved through an expanded isotope list.

A modest change to the 80-isotope list was made with the addition of 5 isotopes; the results of this change are shown in figure 3. Significant improve-

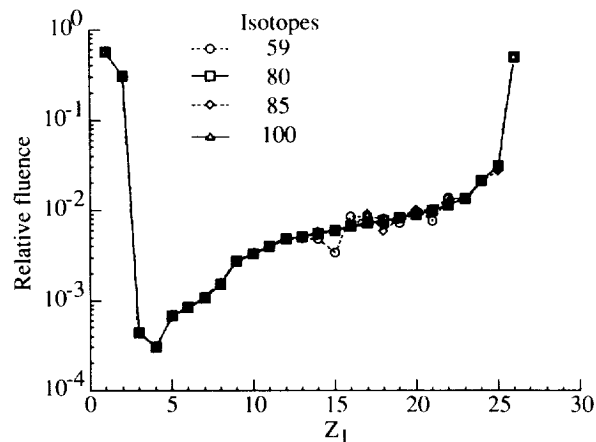


Figure 4. Convergence of charge distribution of 505 MeV/amu iron beams in 5 g/cm² of epoxy for 59, 80, 85, and 100 isotopes.

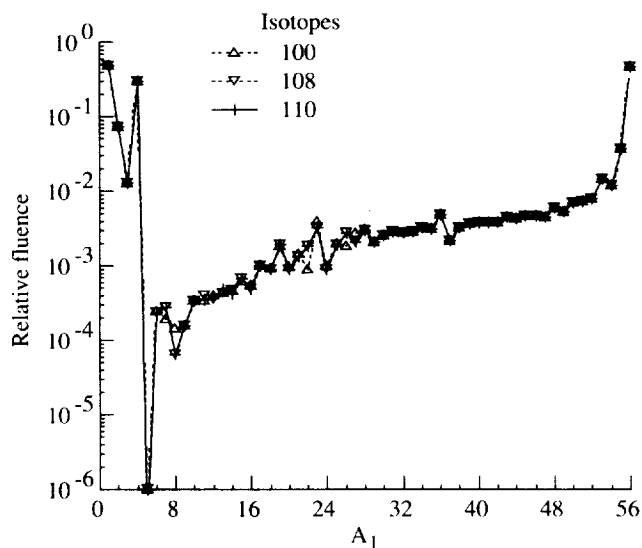


Figure 5. Convergence of mass distribution of 505 MeV/amu iron beams in 5 g/cm² of epoxy for 100, 108, and 110 isotopes.

ment in the mass distribution is achieved for $A_l < 40$, but the result degrades at higher mass numbers. The charge distribution was less accurate and the use of a 100-isotope list could not adequately resolve the convergence problem for the mass distribution as seen in figures 3 and 4. The isotope tables were incrementally expanded with continuous improvement in the mass distribution, as seen in figures 5–8. The final list of 122 isotopes appears to be the minimum set required to represent the fragment mass distribution. The charge distribution had nearly converged at 80 isotopes and no substantial change in its

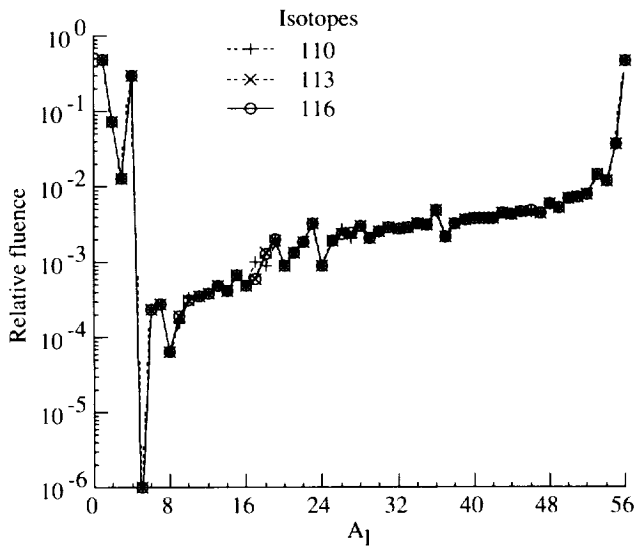


Figure 6. Convergence of mass distribution of 505 MeV/amu iron beams in 5 g/cm² of epoxy for 110, 113, and 116 isotopes.

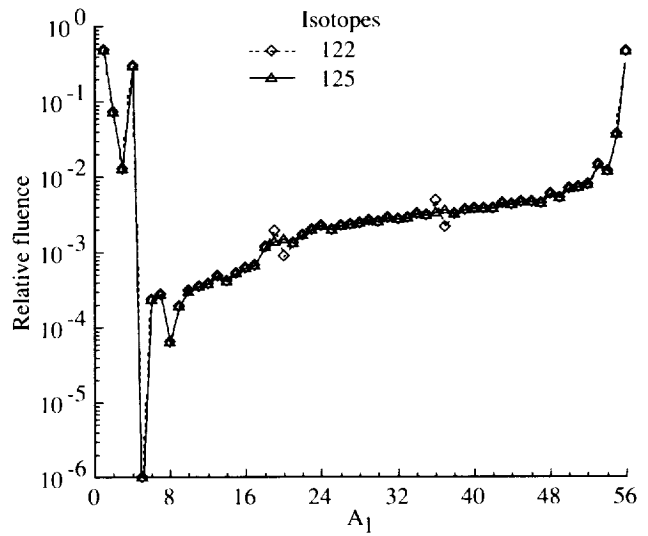


Figure 8. Convergence of mass distribution of 505 MeV/amu iron beams in 5 g/cm² of epoxy for 122 and 125 isotopes.

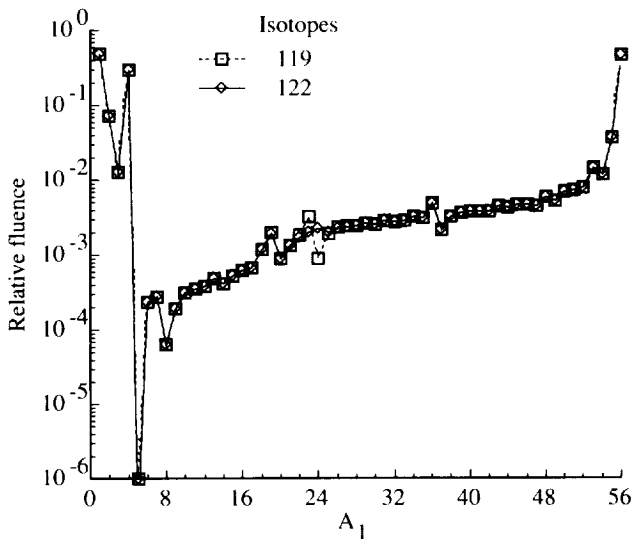


Figure 7. Convergence of mass distribution of 505 MeV/amu iron beams in 5 g/cm² of epoxy for 119 and 122 isotopes.

convergence occurs beyond 100 isotopes, as seen in figure 9.

Although the specific tests were derived for an iron beam on a given epoxy resin, the isotope distributions are largely dominated by the nuclear physics of the projectile fragments and virtually all elements are produced below the projectile atomic number; thus, we expect similar convergence properties for other shield materials. We also note that the iron beam is a principal contributor to galactic cosmic

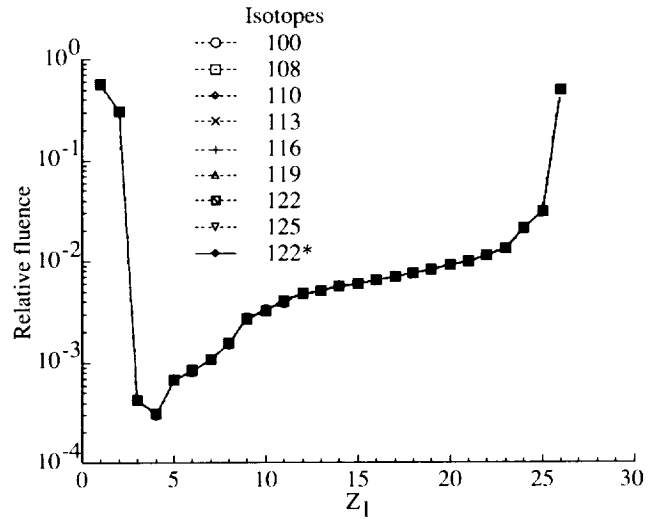


Figure 9. Convergence of charge distribution of 505 MeV/amu iron beams in 5 g/cm² of epoxy for 100 isotopes and greater.

ray exposure and the current results indicate that the space shield calculations require a larger table than the 59 isotopes currently listed.

Discussion of Results

Computational precision of charge and mass distribution is provided by adding more isotopes to the table. However, each additional isotope requires additional computation time to generate the non-perturbative Green's functions for the selected isotope table. An optimal choice of isotope table is

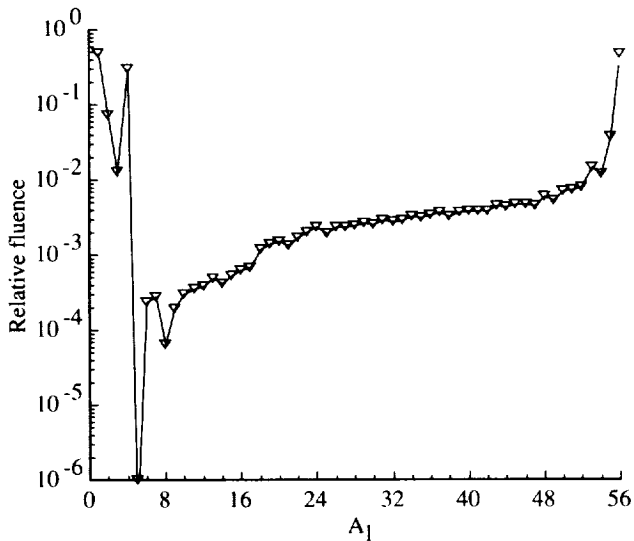


Figure 10. Mass distribution of 505 MeV/amu iron beams in 5 g/cm² of epoxy for revised table with 122 isotopes.

needed for both computational precision and practical computation time.

The detailed isotope selections are shown in tables I and II. Figures 8, 9, and 10 show that an optimal choice is the revised table of 122 isotopes. (See table II and attendant footnote.) In figures 8 and 10, the integral output spectra converge within 5 percent compared with the 125-isotope list over the entire projectile fragment nuclear mass range of 1 to 56. In figure 9, integral output spectra are plotted over the charge range of 1 to 26, where the maximum difference is within 2.7 percent over the entire projectile fragment nuclei range for tables with 100 or more isotopes. A similar plot for 80 isotopes (fig. 1) gives a maximum difference of 3.1 percent. Although the largest list considered (125 isotopes) may not be fully converged, we believe that the error introduced by the 125-isotope list is much less than 5 percent in mass and 2 percent in charge distribution.

Concluding Remarks

Improvements in the treatment of the nuclear database are required so that space radiation codes will agree well with experiments. The improvement addressed in this research was the determination of an optimal isotope table to generate the nuclear database that gives both computational precision and practical computation time. An iron beam in epoxy was chosen to study the effects of isotope list selection on the mass and charge distributions of the transmitted fluence computed by nonperturbative methods in the transport of high-charge and high-energy ions. A table of 80 isotopes gives charge versus flu-

ence spectra that converge within 3.1 percent; a table of 100 isotopes converges within 2.7 percent. A table of 122 isotopes gives nuclear mass versus fluence spectra that converge within 5 percent. These tables also result in practical computation times. Iron is the most abundant massive ion in space and the fragmentation event is dominated by the nuclear structure of the projectiles, so these results are generally applicable to other materials and ions important to the space radiation problem.

References

1. Wilson, John W.; Badavi, Francis F.; Costen, Robert C.; and Shinn, Judy L.: *Nonperturbative Methods in HZE Ion Transport*. NASA TP-3363, 1993.
2. Schimmerling, Walter; Miller, Jack; Wong, Mervyn; Rapkin, Marwin; Howard, Jerry; Spieler, Helmut G.; and Jarret, Blair V.: The Fragmentation of 670A MeV Neon-20 as a Function of Depth in Water. *Radiat. Res.*, vol. 120, 1989, pp. 36-71.
3. Shavers, Mark R.; Curtis, Stanley B.; Miller, Jack; and Schimmerling, Walter: The Fragmentation of 670A MeV Neon-20 as a Function of Depth in Water. II. One-Generation Transport Theory. *Radiat. Res.*, vol. 124, 1990, pp. 117-130.
4. Wilson, John W.; Townsend, Lawrence W.; and Badavi, F. F.: A Semiempirical Nuclear Fragmentation Model. *Nucl. Instrum. & Methods Phys. Res.*, vol. B18, no. 3, Feb. 1987, pp. 225-231.
5. Shinn, Judy L.; John, Sarah; Tripathi, Ram K.; Wilson, John W.; Townsend, Lawrence W.; and Norbury, John W.: *Fully Energy-Dependent HZETRN (A Galactic Cosmic-Ray Transport Code)*. NASA TP-3243, 1992.
6. Wilson, J. W.; and Badavi, F. F.: New Directions in Heavy Ion Shielding. *Proceedings of the Topical Meeting on New Horizons in Radiation Protection and Shielding*, American Nuclear Soc., Inc., 1992, pp. 205-211.
7. Curtis, S. B.; Doherty, W. R.; and Wilkinson, M. C.: *Study of Radiation Hazards to Man on Extended Near Earth Missions*. NASA CR-1469, 1969.
8. Letaw, John; Tsao, C. H.; and Silberberg, R.: Matrix Methods of Cosmic Ray Propagation. *Composition and Origin of Cosmic Rays*, Maurice M. Shapiro, ed., D. Reidel Publ. Co., 1983, pp. 337-342.
9. Wilson, John W.; Townsend, Lawrence W.; Schimmerling, Walter; Khandelwal, Govind S.; Khan, Ferdous; Nealy, John E.; Cucinotta, Francis A.; Simonsen, Lisa C.; Shinn, Judy L.; and Norbury, John W.: *Transport Methods and Interactions for Space Radiations*. NASA RP-1257, 1991.
10. Cucinotta, Francis A.: *Calculations of Cosmic-Ray Helium Transport in Shielding Materials*. NASA TP-3354, 1993.

Table I. Detailed Index for Isotopes 59-110

Z	Number of isotopes					
	59	80	85	100	108	110
0	¹ n	¹ n	¹ n	¹ n	¹ n	¹ n
1	¹ H	¹ H	¹ H	¹ H	¹ H	¹ H
	² H	² H	² H	² H	² H	² H
	³ H	³ H	³ H	³ H	³ H	³ H
2	³ He	³ He	³ He	³ He	³ He	³ He
	⁴ He	⁴ He	⁴ He	⁴ He	⁴ He	⁴ He
3	⁶ Li	⁶ Li	⁶ Li	⁶ Li	⁶ Li	⁶ Li
	⁷ Li	⁷ Li	⁷ Li	⁷ Li	⁷ Li	⁷ Li
4					⁷ Be	⁷ Be
	⁸ Be	⁸ Be	⁸ Be	⁸ Be	⁸ Be	⁸ Be
	⁹ Be	⁹ Be	⁹ Be	⁹ Be	⁹ Be	⁹ Be
5	¹⁰ B	¹⁰ B	¹⁰ B	¹⁰ B	¹⁰ B	¹⁰ B
	¹¹ B	¹¹ B	¹¹ B	¹¹ B	¹¹ B	¹¹ B
						¹² B
6					¹¹ C	¹¹ C
	¹² C	¹² C	¹² C	¹² C	¹² C	¹² C
	¹³ C	¹³ C	¹³ C	¹³ C	¹³ C	¹³ C
7						¹³ N
	¹⁴ N	¹⁴ N	¹⁴ N	¹⁴ N	¹⁴ N	¹⁴ N
	¹⁵ N	¹⁵ N	¹⁵ N	¹⁵ N	¹⁵ N	¹⁵ N
8					¹⁵ O	¹⁵ O
	¹⁶ O	¹⁶ O	¹⁶ O	¹⁶ O	¹⁶ O	¹⁶ O
	¹⁷ O	¹⁷ O	¹⁷ O	¹⁷ O	¹⁷ O	¹⁷ O
9	¹⁸ F	¹⁸ F	¹⁸ F	¹⁸ F	¹⁸ F	¹⁸ F
	¹⁹ F	¹⁹ F	¹⁹ F	¹⁹ F	¹⁹ F	¹⁹ F
10					¹⁹ Ne	¹⁹ Ne
	²⁰ Ne	²⁰ Ne	²⁰ Ne	²⁰ Ne	²⁰ Ne	²⁰ Ne
	²¹ Ne	²¹ Ne	²¹ Ne	²¹ Ne	²¹ Ne	²¹ Ne
	²² Ne	²² Ne	²² Ne	²² Ne	²² Ne	²² Ne
11					²² Na	²² Na
	²³ Na	²³ Na	²³ Na	²³ Na	²³ Na	²³ Na
12					²³ Mg	²³ Mg
	²⁴ Mg	²⁴ Mg	²⁴ Mg	²⁴ Mg	²⁴ Mg	²⁴ Mg
	²⁵ Mg	²⁵ Mg	²⁵ Mg	²⁵ Mg	²⁵ Mg	²⁵ Mg
	²⁶ Mg	²⁶ Mg	²⁶ Mg	²⁶ Mg	²⁶ Mg	²⁶ Mg
13					²⁶ Al	²⁶ Al
	²⁷ Al	²⁷ Al	²⁷ Al	²⁷ Al	²⁷ Al	²⁷ Al
		²⁸ Al	²⁸ Al	²⁸ Al	²⁸ Al	²⁸ Al

Table I. Concluded

Z	Number of isotopes					
	59	80	85	100	108	110
20	⁴⁰ Ca	⁴⁰ Ca	⁴⁰ Ca	⁴⁰ Ca	⁴⁰ Ca	⁴⁰ Ca
	⁴¹ Ca	⁴¹ Ca	⁴¹ Ca	⁴¹ Ca	⁴¹ Ca	⁴¹ Ca
	⁴² Ca	⁴² Ca	⁴² Ca	⁴² Ca	⁴² Ca	⁴² Ca
		⁴³ Ca	⁴³ Ca	⁴³ Ca	⁴³ Ca	⁴³ Ca
			⁴⁴ Ca	⁴⁴ Ca	⁴⁴ Ca	⁴⁴ Ca
			⁴⁵ Ca	⁴⁵ Ca	⁴⁵ Ca	⁴⁵ Ca
21	⁴³ Sc	⁴³ Sc		⁴³ Sc	⁴³ Sc	⁴³ Sc
		⁴⁴ Sc		⁴⁴ Sc	⁴⁴ Sc	⁴⁴ Sc
		⁴⁵ Sc	⁴⁵ Sc	⁴⁵ Sc	⁴⁵ Sc	⁴⁵ Sc
		⁴⁶ Sc	⁴⁶ Sc	⁴⁶ Sc	⁴⁶ Sc	⁴⁶ Sc
			⁴⁷ Sc	⁴⁷ Sc	⁴⁷ Sc	⁴⁷ Sc
			⁴⁸ Sc	⁴⁸ Sc	⁴⁸ Sc	⁴⁸ Sc
22	⁴⁴ Ti	⁴⁴ Ti		⁴⁴ Ti	⁴⁴ Ti	⁴⁴ Ti
	⁴⁵ Ti	⁴⁵ Ti		⁴⁵ Ti	⁴⁵ Ti	⁴⁵ Ti
	⁴⁶ Ti	⁴⁶ Ti		⁴⁶ Ti	⁴⁶ Ti	⁴⁶ Ti
	⁴⁷ Ti	⁴⁷ Ti	⁴⁷ Ti	⁴⁷ Ti	⁴⁷ Ti	⁴⁷ Ti
		⁴⁸ Ti	⁴⁸ Ti	⁴⁸ Ti	⁴⁸ Ti	⁴⁸ Ti
		⁴⁹ Ti	⁴⁹ Ti	⁴⁹ Ti	⁴⁹ Ti	⁴⁹ Ti
23	⁴⁸ V	⁴⁸ V		⁴⁸ V	⁴⁸ V	⁴⁸ V
	⁴⁹ V	⁴⁹ V		⁴⁹ V	⁴⁹ V	⁴⁹ V
		⁵⁰ V	⁵⁰ V	⁵⁰ V	⁵⁰ V	⁵⁰ V
		⁵¹ V	⁵¹ V	⁵¹ V	⁵¹ V	⁵¹ V
		⁵² V	⁵² V	⁵² V	⁵² V	⁵² V
24	⁵⁰ Cr	⁵⁰ Cr		⁵⁰ Cr	⁵⁰ Cr	⁵⁰ Cr
	⁵¹ Cr	⁵¹ Cr		⁵¹ Cr	⁵¹ Cr	⁵¹ Cr
	⁵² Cr	⁵² Cr	⁵² Cr	⁵² Cr	⁵² Cr	⁵² Cr
		⁵³ Cr	⁵³ Cr	⁵³ Cr	⁵³ Cr	⁵³ Cr
			⁵⁴ Cr	⁵⁴ Cr	⁵⁴ Cr	⁵⁴ Cr
25	⁵³ Mn	⁵³ Mn		⁵³ Mn	⁵³ Mn	⁵³ Mn
	⁵⁴ Mn	⁵⁴ Mn	⁵⁴ Mn	⁵⁴ Mn	⁵⁴ Mn	⁵⁴ Mn
		⁵⁵ Mn	⁵⁵ Mn	⁵⁵ Mn	⁵⁵ Mn	⁵⁵ Mn
26	⁵⁵ Fe	⁵⁵ Fe	⁵⁵ Fe	⁵⁵ Fe	⁵⁵ Fe	⁵⁵ Fe
	⁵⁶ Fe	⁵⁶ Fe	⁵⁶ Fe	⁵⁶ Fe	⁵⁶ Fe	⁵⁶ Fe
27	⁵⁷ Co	⁵⁷ Co	⁵⁷ Co	⁵⁷ Co	⁵⁷ Co	⁵⁷ Co
28	⁵⁸ Ni	⁵⁸ Ni	⁵⁸ Ni	⁵⁸ Ni	⁵⁸ Ni	⁵⁸ Ni

Table II. Detailed Index for Isotopes 113–125

Z	Number of isotopes					
	113	116	119	122	125	122*
0	¹ n	¹ n	¹ n	¹ n	¹ n	¹ n
1	¹ H	¹ H	¹ H	¹ H	¹ H	¹ H
	² H	² H	² H	² H	² H	² H
	³ H	³ H	³ H	³ H	³ H	³ H
2	³ He	³ He	³ He	³ He	³ He	³ He
	⁴ He	⁴ He	⁴ He	⁴ He	⁴ He	⁴ He
3	⁶ Li	⁶ Li	⁶ Li	⁶ Li	⁶ Li	⁶ Li
	⁷ Li	⁷ Li	⁷ Li	⁷ Li	⁷ Li	⁷ Li
4	⁷ Be	⁷ Be	⁷ Be	⁷ Be	⁷ Be	⁷ Be
	⁸ Be	⁸ Be	⁸ Be	⁸ Be	⁸ Be	⁸ Be
	⁹ Be	⁹ Be	⁹ Be	⁹ Be	⁹ Be	⁹ Be
5			⁸ B			
	⁹ B	⁹ B	⁹ B	⁹ B	⁹ B	⁹ B
	¹⁰ B	¹⁰ B	¹⁰ B	¹⁰ B	¹⁰ B	¹⁰ B
	¹¹ B	¹¹ B	¹¹ B	¹¹ B	¹¹ B	¹¹ B
	¹² B	¹² B	¹² B	¹² B	¹² B	¹² B
6	¹¹ C	¹¹ C	¹¹ C	¹¹ C	¹¹ C	¹¹ C
	¹² C	¹² C	¹² C	¹² C	¹² C	¹² C
	¹³ C	¹³ C	¹³ C	¹³ C	¹³ C	¹³ C
7	¹³ N	¹³ N	¹³ N	¹³ N	¹³ N	¹³ N
	¹⁴ N	¹⁴ N	¹⁴ N	¹⁴ N	¹⁴ N	¹⁴ N
	¹⁵ N	¹⁵ N	¹⁵ N	¹⁵ N	¹⁵ N	¹⁵ N
			¹⁶ N	¹⁶ N	¹⁶ N	¹⁶ N
8	¹⁵ O	¹⁵ O	¹⁵ O	¹⁵ O	¹⁵ O	¹⁵ O
	¹⁶ O	¹⁶ O	¹⁶ O	¹⁶ O	¹⁶ O	¹⁶ O
	¹⁷ O	¹⁷ O	¹⁷ O	¹⁷ O	¹⁷ O	¹⁷ O
	¹⁸ O	¹⁸ O	¹⁸ O	¹⁸ O	¹⁸ O	¹⁸ O
		¹⁹ O	¹⁹ O	¹⁹ O	¹⁹ O	¹⁹ O
9			¹⁷ F	¹⁷ F	¹⁷ F	¹⁷ F
	¹⁸ F	¹⁸ F	¹⁸ F	¹⁸ F	¹⁸ F	¹⁸ F
	¹⁹ F	¹⁹ F	¹⁹ F	¹⁹ F	¹⁹ F	¹⁹ F
					²⁰ F	²⁰ F
10	¹⁹ Ne	¹⁹ Ne	¹⁹ Ne	¹⁹ Ne	¹⁹ Ne	¹⁹ Ne
	²⁰ Ne	²⁰ Ne	²⁰ Ne	²⁰ Ne	²⁰ Ne	²⁰ Ne
	²¹ Ne	²¹ Ne	²¹ Ne	²¹ Ne	²¹ Ne	²¹ Ne
	²² Ne	²² Ne	²² Ne	²² Ne	²² Ne	²² Ne
11				²³ Ne	²³ Ne	²³ Ne
	²² Na	²² Na	²² Na	²² Na	²² Na	²² Na
	²³ Na	²³ Na	²³ Na	²³ Na	²³ Na	²³ Na
				²⁴ Na	²⁴ Na	²⁴ Na

*Resulting 122-isotope list that is adequate for ion beams.

Table II. Continued

Z	Number of isotopes					
	113	116	119	122	125	122*
12				²² Mg	²² Mg	
	²³ Mg	²³ Mg	²³ Mg	²³ Mg	²³ Mg	²³ Mg
	²⁴ Mg	²⁴ Mg	²⁴ Mg	²⁴ Mg	²⁴ Mg	²⁴ Mg
	²⁵ Mg	²⁵ Mg	²⁵ Mg	²⁵ Mg	²⁵ Mg	²⁵ Mg
	²⁶ Mg	²⁶ Mg	²⁶ Mg	²⁶ Mg	²⁶ Mg	²⁶ Mg
	²⁷ Mg	²⁷ Mg	²⁷ Mg	²⁷ Mg	²⁷ Mg	²⁷ Mg
13			²⁸ Mg	²⁸ Mg	²⁸ Mg	²⁸ Mg
				²⁵ Al	²⁵ Al	
	²⁶ Al	²⁶ Al	²⁶ Al	²⁶ Al	²⁶ Al	²⁶ Al
	²⁷ Al	²⁷ Al	²⁷ Al	²⁷ Al	²⁷ Al	²⁷ Al
	²⁸ Al	²⁸ Al	²⁸ Al	²⁸ Al	²⁸ Al	²⁸ Al
			²⁹ Al	²⁹ Al	²⁹ Al	²⁹ Al
14	²⁷ Si	²⁷ Si	²⁷ Si	²⁷ Si	²⁷ Si	²⁷ Si
	²⁸ Si	²⁸ Si	²⁸ Si	²⁸ Si	²⁸ Si	²⁸ Si
	²⁹ Si	²⁹ Si	²⁹ Si	²⁹ Si	²⁹ Si	²⁹ Si
	³⁰ Si	³⁰ Si	³⁰ Si	³⁰ Si	³⁰ Si	³⁰ Si
	³¹ Si	³¹ Si	³¹ Si	³¹ Si	³¹ Si	³¹ Si
15	²⁹ P	²⁹ P	²⁹ P	²⁹ P	²⁹ P	²⁹ P
	³⁰ P	³⁰ P	³⁰ P	³⁰ P	³⁰ P	³⁰ P
	³¹ P	³¹ P	³¹ P	³¹ P	³¹ P	³¹ P
	³² P	³² P	³² P	³² P	³² P	³² P
	³³ P	³³ P	³³ P	³³ P	³³ P	³³ P
	³⁴ P	³⁴ P	³⁴ P	³⁴ P	³⁴ P	³⁴ P
16	³¹ S	³¹ S	³¹ S	³¹ S	³¹ S	³¹ S
	³² S	³² S	³² S	³² S	³² S	³² S
	³³ S	³³ S	³³ S	³³ S	³³ S	³³ S
	³⁴ S	³⁴ S	³⁴ S	³⁴ S	³⁴ S	³⁴ S
	³⁵ S	³⁵ S	³⁵ S	³⁵ S	³⁵ S	³⁵ S
	³⁶ S	³⁶ S	³⁶ S	³⁶ S	³⁶ S	³⁶ S
	³⁷ S	³⁷ S	³⁷ S	³⁷ S	³⁷ S	³⁷ S
17		³⁸ S				
	³⁴ Cl	³⁴ Cl	³⁴ Cl	³⁴ Cl	³⁴ Cl	³⁴ Cl
	³⁵ Cl	³⁵ Cl	³⁵ Cl	³⁵ Cl	³⁵ Cl	³⁵ Cl
	³⁶ Cl	³⁶ Cl	³⁶ Cl	³⁶ Cl	³⁶ Cl	³⁶ Cl
	³⁷ Cl	³⁷ Cl	³⁷ Cl	³⁷ Cl	³⁷ Cl	³⁷ Cl
	³⁸ Cl	³⁸ Cl	³⁸ Cl	³⁸ Cl	³⁸ Cl	³⁸ Cl
18	³⁹ Cl	³⁹ Cl	³⁹ Cl	³⁹ Cl	³⁹ Cl	³⁹ Cl
	³⁶ Ar	³⁶ Ar	³⁶ Ar	³⁶ Ar	³⁶ Ar	³⁶ Ar
					³⁷ Ar	³⁷ Ar
	³⁸ Ar	³⁸ Ar	³⁸ Ar	³⁸ Ar	³⁸ Ar	³⁸ Ar
	³⁹ Ar	³⁹ Ar	³⁹ Ar	³⁹ Ar	³⁹ Ar	³⁹ Ar
	⁴⁰ Ar	⁴⁰ Ar	⁴⁰ Ar	⁴⁰ Ar	⁴⁰ Ar	⁴⁰ Ar
	⁴¹ Ar	⁴¹ Ar	⁴¹ Ar	⁴¹ Ar	⁴¹ Ar	⁴¹ Ar
	⁴² Ar	⁴² Ar	⁴² Ar	⁴² Ar	⁴² Ar	⁴² Ar

*Resulting 122-isotope list that is adequate for ion beams.

Table II. Concluded

Z	Number of isotopes					
	113	116	119	122	125	122*
19	³⁷ K	³⁷ K	³⁷ K	³⁷ K	³⁷ K	³⁷ K
	³⁹ K	³⁹ K	³⁹ K	³⁹ K	³⁹ K	³⁹ K
	⁴⁰ K	⁴⁰ K	⁴⁰ K	⁴⁰ K	⁴⁰ K	⁴⁰ K
	⁴¹ K	⁴¹ K	⁴¹ K	⁴¹ K	⁴¹ K	⁴¹ K
	⁴² K	⁴² K	⁴² K	⁴² K	⁴² K	⁴² K
	⁴³ K	⁴³ K	⁴³ K	⁴³ K	⁴³ K	⁴³ K
20	⁴⁰ Ca	⁴⁰ Ca	⁴⁰ Ca	⁴⁰ Ca	⁴⁰ Ca	⁴⁰ Ca
	⁴¹ Ca	⁴¹ Ca	⁴¹ Ca	⁴¹ Ca	⁴¹ Ca	⁴¹ Ca
	⁴² Ca	⁴² Ca	⁴² Ca	⁴² Ca	⁴² Ca	⁴² Ca
	⁴³ Ca	⁴³ Ca	⁴³ Ca	⁴³ Ca	⁴³ Ca	⁴³ Ca
	⁴⁴ Ca	⁴⁴ Ca	⁴⁴ Ca	⁴⁴ Ca	⁴⁴ Ca	⁴⁴ Ca
	⁴⁵ Ca	⁴⁵ Ca	⁴⁵ Ca	⁴⁵ Ca	⁴⁵ Ca	⁴⁵ Ca
21	⁴³ Sc	⁴³ Sc	⁴³ Sc	⁴³ Sc	⁴³ Sc	⁴³ Sc
	⁴⁴ Sc	⁴⁴ Sc	⁴⁴ Sc	⁴⁴ Sc	⁴⁴ Sc	⁴⁴ Sc
	⁴⁵ Sc	⁴⁵ Sc	⁴⁵ Sc	⁴⁵ Sc	⁴⁵ Sc	⁴⁵ Sc
	⁴⁶ Sc	⁴⁶ Sc	⁴⁶ Sc	⁴⁶ Sc	⁴⁶ Sc	⁴⁶ Sc
	⁴⁷ Sc	⁴⁷ Sc	⁴⁷ Sc	⁴⁷ Sc	⁴⁷ Sc	⁴⁷ Sc
	⁴⁸ Sc	⁴⁸ Sc	⁴⁸ Sc	⁴⁸ Sc	⁴⁸ Sc	⁴⁸ Sc
22	⁴⁴ Ti	⁴⁴ Ti	⁴⁴ Ti	⁴⁴ Ti	⁴⁴ Ti	⁴⁴ Ti
	⁴⁵ Ti	⁴⁵ Ti	⁴⁵ Ti	⁴⁵ Ti	⁴⁵ Ti	⁴⁵ Ti
	⁴⁶ Ti	⁴⁶ Ti	⁴⁶ Ti	⁴⁶ Ti	⁴⁶ Ti	⁴⁶ Ti
	⁴⁷ Ti	⁴⁷ Ti	⁴⁷ Ti	⁴⁷ Ti	⁴⁷ Ti	⁴⁷ Ti
	⁴⁸ Ti	⁴⁸ Ti	⁴⁸ Ti	⁴⁸ Ti	⁴⁸ Ti	⁴⁸ Ti
	⁴⁹ Ti	⁴⁹ Ti	⁴⁹ Ti	⁴⁹ Ti	⁴⁹ Ti	⁴⁹ Ti
23	⁵⁰ Ti	⁵⁰ Ti	⁵⁰ Ti	⁵⁰ Ti	⁵⁰ Ti	⁵⁰ Ti
	⁴⁸ V	⁴⁸ V	⁴⁸ V	⁴⁸ V	⁴⁸ V	⁴⁸ V
	⁴⁹ V	⁴⁹ V	⁴⁹ V	⁴⁹ V	⁴⁹ V	⁴⁹ V
	⁵⁰ V	⁵⁰ V	⁵⁰ V	⁵⁰ V	⁵⁰ V	⁵⁰ V
	⁵¹ V	⁵¹ V	⁵¹ V	⁵¹ V	⁵¹ V	⁵¹ V
24	⁵² V	⁵² V	⁵² V	⁵² V	⁵² V	⁵² V
	⁵⁰ Cr	⁵⁰ Cr	⁵⁰ Cr	⁵⁰ Cr	⁵⁰ Cr	⁵⁰ Cr
	⁵¹ Cr	⁵¹ Cr	⁵¹ Cr	⁵¹ Cr	⁵¹ Cr	⁵¹ Cr
	⁵² Cr	⁵² Cr	⁵² Cr	⁵² Cr	⁵² Cr	⁵² Cr
	⁵³ Cr	⁵³ Cr	⁵³ Cr	⁵³ Cr	⁵³ Cr	⁵³ Cr
25	⁵⁴ Cr	⁵⁴ Cr	⁵⁴ Cr	⁵⁴ Cr	⁵⁴ Cr	⁵⁴ Cr
	⁵³ Mn	⁵³ Mn	⁵³ Mn	⁵³ Mn	⁵³ Mn	⁵³ Mn
	⁵⁴ Mn	⁵⁴ Mn	⁵⁴ Mn	⁵⁴ Mn	⁵⁴ Mn	⁵⁴ Mn
26	⁵⁵ Mn	⁵⁵ Mn	⁵⁵ Mn	⁵⁵ Mn	⁵⁵ Mn	⁵⁵ Mn
	⁵⁵ Fe	⁵⁵ Fe	⁵⁵ Fe	⁵⁵ Fe	⁵⁵ Fe	⁵⁵ Fe
27	⁵⁶ Fe	⁵⁶ Fe	⁵⁶ Fe	⁵⁶ Fe	⁵⁶ Fe	⁵⁶ Fe
	⁵⁷ Co	⁵⁷ Co	⁵⁷ Co	⁵⁷ Co	⁵⁷ Co	⁵⁷ Co
28	⁵⁸ Ni	⁵⁸ Ni	⁵⁸ Ni	⁵⁸ Ni	⁵⁸ Ni	⁵⁸ Ni

*Resulting 122-isotope list that is adequate for ion beams.

REPORT DOCUMENTATION PAGE			Form Approved OMB No. 0704-0188	
Public reporting burden for this collection of information is estimated to average 1 hour per response, including the time for reviewing instructions, searching existing data sources, gathering and maintaining the data needed, and completing and reviewing the collection of information. Send comments regarding this burden estimate or any other aspect of this collection of information, including suggestions for reducing this burden, to Washington Headquarters Services, Directorate for Information Operations and Reports, 1215 Jefferson Davis Highway, Suite 1204, Arlington, VA 22202-4302, and to the Office of Management and Budget, Paperwork Reduction Project (0704-0188), Washington, DC 20503.				
1. AGENCY USE ONLY (Leave blank)	2. REPORT DATE May 1994	3. REPORT TYPE AND DATES COVERED Technical Paper		
4. TITLE AND SUBTITLE Effects of Isotope Selection on Solution Convergence in HZE Transport		5. FUNDING NUMBERS WU 199-45-16-11		
6. AUTHOR(S) Myung-Hee Y. Kim, John W. Wilson, Richard L. Kiefer, and Sheila A. Thibeault				
7. PERFORMING ORGANIZATION NAME(S) AND ADDRESS(ES) NASA Langley Research Center Hampton, VA 23681-0001		8. PERFORMING ORGANIZATION REPORT NUMBER L-17357		
9. SPONSORING/MONITORING AGENCY NAME(S) AND ADDRESS(ES) National Aeronautics and Space Administration Washington, DC 20546-0001		10. SPONSORING/MONITORING AGENCY REPORT NUMBER NASA TP-3445		
11. SUPPLEMENTARY NOTES Kim and Kiefer: The College of William and Mary, Williamsburg, Virginia; Wilson and Thibeault: Langley Research Center, Hampton, Virginia.				
12a. DISTRIBUTION/AVAILABILITY STATEMENT Unclassified-Unlimited Subject Category 93		12b. DISTRIBUTION CODE		
13. ABSTRACT (Maximum 200 words) A fragmenting iron ion produces hundreds of isotopes during nuclear reactions. These isotopes are represented in the solution of the transport problem. A reduced set of isotopes is selected to minimize the computational burden but introduces error in the final result. A minimum list of 122 isotopes is required for adequate representation of the mass and charge distributions of the secondary radiation fields. A reduced set of 80 isotopes is sufficient to represent the charge distribution alone and represents reasonably well the linear energy transfer properties of the iron beam. Because iron fragmentation produces nearly every isotope lighter than iron, the resulting 122-isotope list should be adequate for ion beams with charges equal to or less than 26.				
14. SUBJECT TERMS Radiation protection; Ion beams; Nuclear reactions		15. NUMBER OF PAGES 13		
		16. PRICE CODE A03		
17. SECURITY CLASSIFICATION OF REPORT Unclassified	18. SECURITY CLASSIFICATION OF THIS PAGE Unclassified	19. SECURITY CLASSIFICATION OF ABSTRACT	20. LIMITATION OF ABSTRACT	